ROBUST RECONSTRUCTION OF THE TOPOGRAPHY OF METAL ADDITIVE SURFACES BASED ON FOCUS VARIATION MICROSCOPY

Xin Xu[1], Tobias Pahl[1], Hüseyin Serbes[1], Peter Lehmann[1]
[1]Universität Kassel, Wilhelmshöher Allee 71, 34121 Kassel, Germany

ABSTRACT

When using an optical profiler to measure rough surfaces, especially surfaces generated by metal additive manufacturing, topographical artifacts such as spikes on a reconstructed surface are nearly unavoidable. These may affect the determination of roughness parameters of the topography and lead to erroneous surface features. This paper proposes a new preprocessing method to eliminate most artifacts before extracting surface heights of rough surfaces measured by focus variation microscopy. In this method, the axial region where a surface height value is located with highest probability is estimated, based on datasets of planes parallel to the axial scanning direction. Results regarding height measurements with and without the proposed method are compared by measuring a Rubert Microsurf 329 comparator test panel for reference and a workpiece produced by metal additive manufacturing.

Keywords: focus variation, method, algorithm, profilometry, 3D, measurement, roughness, comparison

1. INTRODUCTION

Metal additive manufacturing (MA) techniques play an important role nowadays in many industrial fields due to their rapid manufacturing process and the capability of complex designs [1]. With the purpose of quality control and process investigation, surface topography measurement becomes more and more important in this context. However, due to the characteristics of the manufacturing process MA generates surfaces with high irregularity and roughness. Surface features such as sharp protrusions, deep recesses, or critical undercuts are difficult to measure [2, 3].

Focus variation microscopy (FVM) is an optical method that reconstructs a surface topography by measuring the axial focus position with respect to each single pixel of a CCD/CMOS camera. The corresponding system scans the measured surface along the optical axis of the objective lens in order to obtain a series of images, named an image stack. It has a limited depth of field (DOF), that is much smaller than the scanning range. As a result, the sub-image around each pixel undergoes a process from defocus to focus and back to defocus again. The focus position is obtained when the corresponding sub-image is sharp with regard to the highest intensity contrast. Therefore, FVM requires a certain minimum roughness of the surface and, thus, it is a good choice to measure MA surfaces. Different foci of individual pixels are obtained at different depth levels in the image stack. As a result, focus detection gives information about the corresponding depth level and the surface topography can be reconstructed [2, 5-7].

Conventional approaches to detect the focus position for a pixel calculate the intensity contrast of neighboring pixels inside a subarea centered by a single pixel. This operation is repeated laterally and shifts the subarea pixel by pixel through the whole image. It is extended to each image of the whole image stack. Therefore, along the scanning direction, a set of contrast values with respect to a single pixel is obtained. The position where the maximum contrast occurs is the measured focus of that pixel [4, 13-15]. Among the common methods for focus detection, the Laplace [8-10, 14], the Tenengrad [11, 12, 15] and the variance focus measure are most commonly used [10]. Modified versions of Laplacian operation are studied in many works. For instance, squaring the second derivative increases the performance [10]. The Tenengrad method squares the results obtained from two perpendicular dimensional Sobel operators prior to a summation, to improve the robustness further. The variance focus measure method calculates the contrast as the standard deviation of intensities with respect to neighboring pixels of a central pixel.

In contrast to conventional methods where the whole image stack is used for detecting the focus, this paper introduces a method, where only the dataset of a partial image stack is used. Such datasets of the whole image stack are obtained by a preprocessing algorithm. In the preprocess, data on planes which are parallel to the axial scanning direction are used to calculate boundaries limiting the most probable focus regions. The most direct advantage is that it effectively reduces or eliminates artifacts which typically appear as spikes. Inside of the focus regions, common methods (standard deviation, Laplacian method, Tenengrad method) to detect the focus position are still used. After investigating several methods in terms of AM workpieces for this paper, the standard deviation method turned out as the best choice due to its superior performance, since this method provides less artifacts in the topography and short computation times compared to the others. Therefore, the method proposed in this paper will be introduced based on the standard deviation method. For convenience we use the terms "proposed method" and "conventional method" throughout this paper, representing the methods with and without preprocessing, respectively.

2. SENSOR SETUP

The experimental setup and a simplified sketch of the FVM with respect to this paper are shown in Figure 1 (a) and (b), respectively. An image stack obtained during a depth scanning process is displayed in Figure 1 (c). From an image stack, a series of contrast values of intensities calculated with respect to the neighboring pixels centered by each single pixel form corresponding contrast curves as shown in Figure 1 (d). The height level corresponds to the position where the maximum contrast represented by the standard deviation σ_{max} occurs.

The illumination methods integrated in the system comprise coaxial illumination using a single green LED (λ= 520 nm, P_{max}= 126 mW) and a dome-shaped ring light (λ = 623 nm). An ALLIED VISION GF146B ASG Guppy CCD camera with IEEE 1394a interface and a number of 1280 × 960 effective pixels is used for detection. The field of view (FOV) is about 0.59 × 0.44 mm^2 in our setup using an objective lens of 0.45 numerical aperture (NA). This results in a DOF of 2.7 μm and the lateral resolution is 0.74 μm for the wavelength of 623 nm. The working distance of the objective lens is about 19 mm. Two stepper motor motion controllers SMC100 from Newport Corporation are used for controlling horizontal and vertical movements of the sample substrate. It is possible to stitch several topographies laterally in one direction. For the stitching an overlap of approx. 150 μm is used for the measurement results shown in this paper. Step sizes Δz, defined as the distance between adjacently captured images in an

image stack, are 0.2, and 0.4 μm, respectively. DOF d_z is calculated by $d_z \sim \lambda/NA^2$, where λ is the central wavelength of the illuminating light.
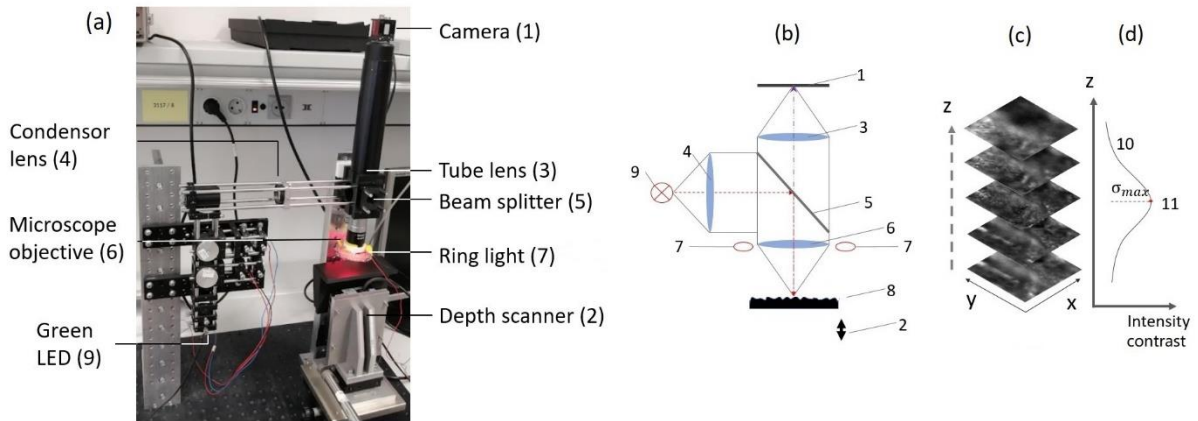

Figure 1. (a) General view of experimental system set up; (b) schematic of experimental system set up; (c) image stack obtained by the camera during the depth scan; (d) intensity contrast curve of a single camera pixel given by the standard deviation of the intensities measured by the surrounding pixels at each vertical position: (1) camera; (2) depth scanner; (3) tube lens; (4) collimator; (5) beam splitter; (6) microscope objective; (7) ring light; (8) workpiece under investigation; (9) LED for coaxial illumination.

3.   METHODOLOGY

3.1   Samples and conventional contrast analysis

The algorithms are compared by measuring a Rubert Microsurf 329 comparator test panel (Figure 2 (a)) and a MA workpiece as shown in Figure 2 (b), respectively. There are 8 sub-areas of 15 mm × 24 mm on the test panel. They are manufactured either by gravel blasting or ball blasting. Because the surface topography produced by gravel blasting has more similarity with the MA workpiece compared to ball blasting, one of the sub-areas named MSS-25 produced by gravel blasting is used for the measurement. The number in the name indicates that its nominal roughness parameter Ra (representing the arithmetic mean value) is 25 μm according to the manufacturer.

For focus detection of a pixel, the conventional method is based on the standard deviation of intensities inside a local area $N \times N$ pixels around this pixel. The calculation of standard deviations is repeated for all images recorded during the depth scan. In contrast to the conventional method in the proposed method only a part of an image stack is needed for focus detection. Commonly, the z-axis corresponds to the depth scanning direction. Therefore, the central pixel position is defined as (x, y, z). A region of foci (foci region) in each $x - z$ plane of an image stack is first searched to select the most probable focus region, where the surface is in focus. This can be seen as a preprocessing.

The standard deviation for a pixel at a certain position (x, y, z) is expressed mathematically by

$$\sigma(k,l,m) = \sqrt{\frac{1}{(2n+1)^2 - 1} \sum_{i=k-n}^{k+n} \sum_{j=l-n}^{l+n} (I(i\Delta x, j\Delta y, m\Delta z) - \bar{I})^2}$$

where $(k\,\Delta x, l\,\Delta y, m\,\Delta z)$ are the coordinates of central pixel inside the window of $N^2 = (2n+1)^2$ pixels; Δx and Δy are the pixel pitches in x and y dimension, respectively; $I(i\,\Delta x, j\,\Delta y, m\,\Delta z)$ with $(i,j) \neq (k,l)$ are the intensities of the neighboring pixels surrounding the central pixel and $\bar{I}$ is the average intensity inside the window [16]. The window size in both, the proposed method and the conventional method is 5×5 pixels, i.e. $n = 2$.
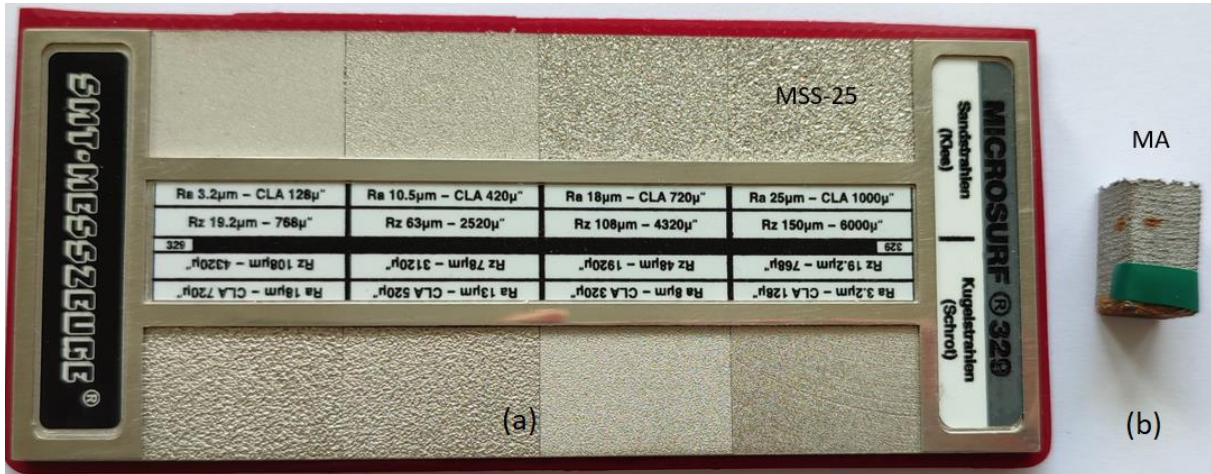

Figure 2. (a) Rubert Microsurf 329 comparator test panel; (b) MA workpiece produced by metal additive manufacturing in the Institute of Materials Engineering at the University of Kassel.

3.2 Proposed Method

Figure 3 (a) and (b) show two images at certain positions taken during the depth scan with respect to MSS-25 and MA correspondingly. Due to the limited DOF only some areas can be observed sharply. At the left lower corner in the image, marked by dashed white square related to MSS-25, there is a small black hole. Due to the low amount of reflected light it is quite difficult to get an image of this hole. Therefore, the surface reconstructed according to the conventional method contains some spikes in this region, as shown in Figure 6 (a1). These spikes are easily detected as artifacts and replaced by interpolated values according to the surrounding measured height values. However, this doesn't work for the area of the MA surface shown in the left lower corner in Figure 3 (b), which is also marked by a dashed white square. The dark areas are located between several small ball-like structures. These areas contain steep slopes and deep holes, which are difficult to be reconstructed. The resulting topography according to the conventional method is shown in Figure 6 (b1). The area of spikes is much bigger compared to Figure 6 (a1). Because the ratio between numbers of spikes and non-spikes inside that area is larger than 50 %, it is hard to distinguish the real shape from artifacts. Therefore, a new method needs to be found to deal with MA surfaces.

Figure 4 (a) shows grey values of a $x - z$ plane obtained by measuring MSS-25. It is related to a column when x is about 3.65 μm, which is crossed with the area marked with the dashed white square in Figure 3 (a). The red curve in this figure represents the reconstructed profile according to the conventional method which contains a sharp spike marked by No.1. This type

of spike can be easily removed, for example by a median filter. However, in Figure 4 (b) there are mainly three artifacts in the surface profile (red curve) according to the conventional method, which are marked by 2, 3, and 4, respectively. Each artifact contains several spikes compared to the single spike in Figure 4 (a). Since these spikes are no longer singular but there is a high ratio of regions with and without spikes, it is not straightforward to identify them as artifacts. Since it is hard to detect these artifacts, it is also not easy to correct or remove them by a median filter either. Therefore, the proposed method is considered in the following.
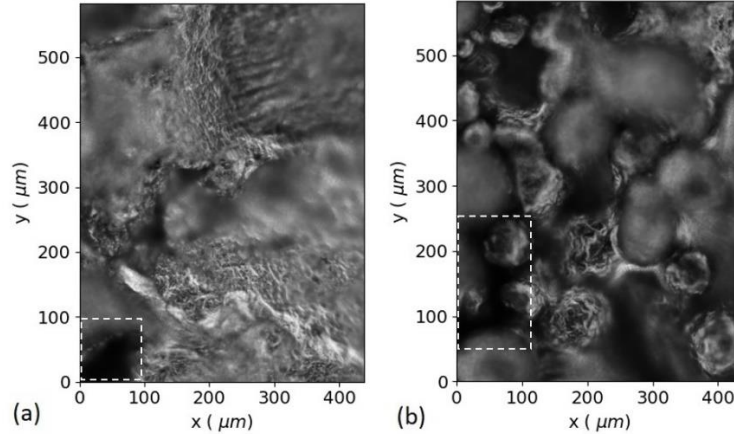

Figure 3. Surface images for certain focus positions of (a) MSS-25 and (b) MA surfaces.

First, it will be shortly introduced, how the proposed method works. The backgrounds in Figure 4 (c) and (d) illustrate the results after applying twice the vertical Sobel operator

$$Sv = \begin{vmatrix} -1 & 0 & 1 \\ -2 & 0 & 2 \\ -1 & 0 & 1 \end{vmatrix}$$

to the images shown in Figure 4 (a) and (b) separately. The Sobel operator is typically used to calculate the gradient of image intensities. It is actually a discrete differentiation operator. The gradient of the intensities at the locations close to foci regions is expected to be higher than in other regions. The purpose of using this operator is to enhance the ability to distinguish the foci regions from others. The results of applying one-time the vertical Sobel operator, twice the horizontal Sobel operator, and the Laplacian operator were compared. The best results are achieved if twice the vertical Sobel operator is used. One benefit of this step is that the foci regions are much better to find in the middle of Figure 4 (c) and (d) compared to Figure 4 (a) and (b). The contrast difference between the foci regions and other regions is higher. In Figure 4 (c) or (d), two boundaries between the foci regions with upper and lower defocus are constructed and illustrated by green and blue curves, respectively. Each boundary separates actually the higher and lower contrast regions. In the end, the focus region of highest probability to detect the correct focus position is obtained. The local standard deviation used in the conventional method as a measure of contrast is only needed inside of these estimated regions instead as for the whole data of the image stack. The boundaries eliminate the spikes which prevent from finding the correct foci. The actual boundaries (green and blue curves) are quite close to each other. They are separated further in order to achieve a better visibility.

In Figure 4 (c), the reason for the appearance of the spike can be explained. The area marked by 'A' indicates a small hole, which might capture most of the light inside of the hole instead of reflecting the light to the camera. In Figure 4 (d), areas 'B', 'C', and 'D' are corresponding to

　　　　　　　5

artefact 2, 3, and 4, respectively. 'B' and 'D' correspond to steep surface slopes and 'C' is a deep hole. Therefore, the amount of light reflected from these areas and received by the camera is not sufficient. Consequently, the contrast values obtained in these regions are less than the contrast values in other defocus regions and thus, spikes appear. The x and z axes are scaled in order to cover the whole profile including the spikes. Therefore, the slope doesn't seem that steep as it actually is. The slope angle is about 55 degrees.
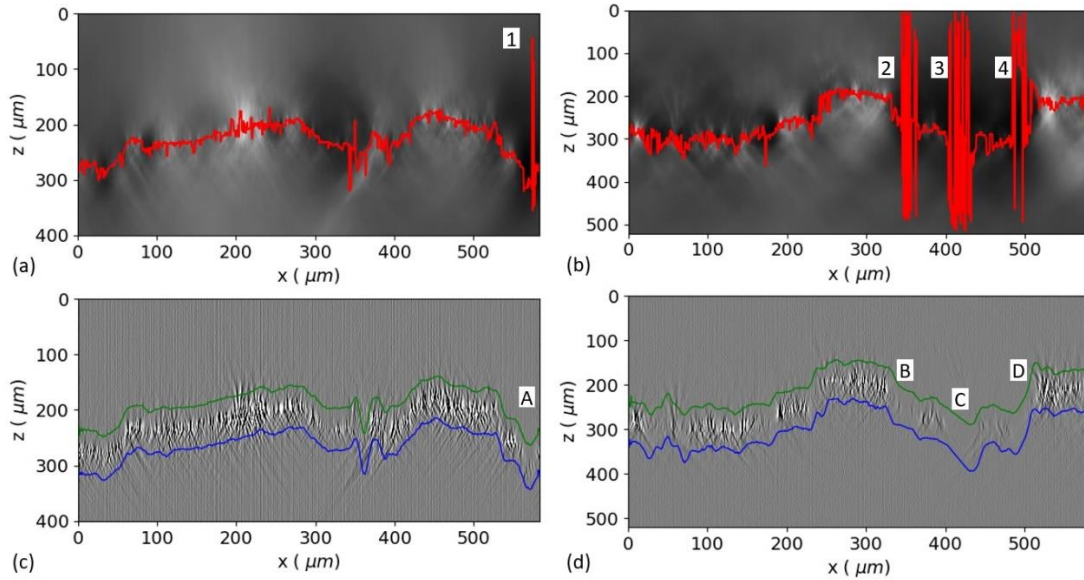

Figure 4. Results after applying the conventional method and illustration of the proposed method: Cross sections for x-z plane in an image stack with the evaluated profile as a red curve using the conventional method with respect to (a) MSS-25 and (b) MA; Results after applying twice the vertical Sobel operator on (a) and (b) separately and two boundaries shown as green and blue curves with respect to (c) MSS-25 and (d) MA.

After the evaluation, the dataset containing the reconstructed topography was imported into the topography analysis software 'Moutains Map' for further processing. For calculating roughness parameters, the FOV of 0.59×0.44 mm^2 is too small. Therefore, 8 reconstructed surface topographies related to the FOV were stitched in order to increase the ROI to approx. 470 µm $\times$ 2.66 mm. Due to the misalignment of the system, the tilt of reconstructed topography is removed first. Then a median filter with a window size of 9×9 pixels is applied. After that, roughness parameters such as Sa (two-dimensional extension of Ra) values are calculated according to ISO 25178 for the whole topography. In ISO standards the required evaluation length is supposed to be 56 mm for a surface with Ra between 10 and 50 µm. However, with the current hardware setup this is impossible. Therefore, only rough evaluation results are shown in this paper and this is one of the reasons of the discrepancies between the Ra values given by the manufacturer and measured values Sa.

4. MEASUREMENT RESULTS

Figure 5 (a) and (b) show the reconstructed profiles (red curves) by the proposed method with respect to Figure 4 (a) and (b) separately. Due to the upper and lower boundaries, the profiles conform to the foci region in the background. The consistency can be also observed by comparing them with Figure 4 (c) and (d), where the foci region is clearer. Even if the recorded roughness in areas A, B, C, and D is weaker than in the surrounding areas, correct focus

positions are still obtained by using the proposed method and, most importantly, the spikes are eliminated.

Table 1 gives the measured Sa value and Ra value as given by the manufacturer with respect to MSS-25, as well as the deviations between them. The results for Ra and Sa values are significant because these are statistical parameters [17]. The deviations between Ra and Sa are 6 %, which indicates the reliability of the proposed method.
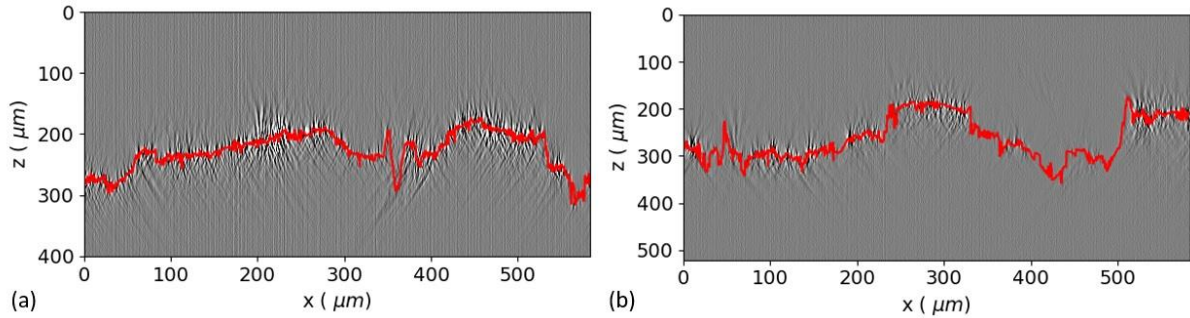

Figure 5. Illustration of the results of profile measurements after applying the proposed method: Cross sections for the x-z plane in an image stack with the reconstructed profiles as red curves for (a) MSS-25 and (b) MA.

Table 1. Comparison of roughness parameters Ra for the Rubert Microsurf 329 comparator test panel and Sa measured by FVM with the proposed method.

	Ra (µm)	Sa (µm)	Deviation of Sa and Ra (%)
MSS-25	25	26.5	6

Figure 6 shows the comparison between the reconstructed topographies with the conventional method and the proposed method. Different heights are indicated by different artificial colors. Figure 6 (a1) and (b1) are the reconstructed surface topographies by applying the conventional method. Figure 6 (a2) and (b2) are the results obtained by use of the proposed method. If the corresponding datasets of Figure 6 (a2) and (b2) are subtracted from Figure 6 (a1) and (b1), Figure 6 (a3) and (b3) result after taking the absolute values. Figure 6 (a1) to (a3) are with respect to MSS-25 and Figure 6 (b1) and (b3) are related to MA. The spike artifacts appearing in Figure 6 (a1) and (b1) disappear in Figure 6 (a2) and (b2). As obtained from the color bars, the maximum height values are significantly reduced by using the proposed method. The difference between Figure 6 (a1) and (a2) is about 171 µm or 42.7 %. The difference between Figure 6 (b1) and (b2) is about 149 µm or 28 %. These height deviations are caused by the spikes. Figure 6 (a3) and (b3) show even clearer where these spikes are located. Therefore, the performance of the proposed method is quite obvious. In addition, to correct the topography shown in Figure 6 (a1) and (b1) obtained by the conventional method needs further postprocessing such as detection and removal of invalid pixels. However, by using the proposed method these two steps can be skipped. More importantly, for the surface shown in Figure 6 (b1) a suitable algorithm to detect the invalid pixels is quite challenging and time consuming.

5. CONCLUSION

In this paper the performance of both, the conventional method and a novel method introduced as 'proposed method' including preprocessing in order to avoid outliers are compared in terms of reconstructing rough surface topographies via FVM. The main difference is the part of the

depth-scanning range used for focus detection at an individual camera pixel. The conventional method requires the entire depth-scanning range, while the proposed method requires only part of it with the help of the preprocessing algorithm. Therefore, the former one suffers from spikes while the latter one eliminates spikes. The proposed method adds a preprocessing step in order to distinguish the foci region from other regions before the main step of the focus detection is carried out. The most obvious advantage of the foci region is that it greatly eliminates or reduces artifacts such as spikes, especially when measuring metal additive surfaces. Two commonly used postprocessing steps in the conventional method, namely detection and removal of invalid pixels, are no longer necessary in the proposed method for most surface topologies. In addition, the application of low illumination intensity is enough for MA surfaces in contrast to the case of using both, low and high illumination intensity, during the depth scan for the conventional method. This includes benefits in both, time and energy savings. There is still potential to develop other methods (e.g. image processing) for preprocessing with the help of the dataset in $x - z$ planes or $y - z$ planes. Furthermore, other image processing methods can be investigated for the purpose of increasing the accuracy and the robustness of the preprocessing algorithm.
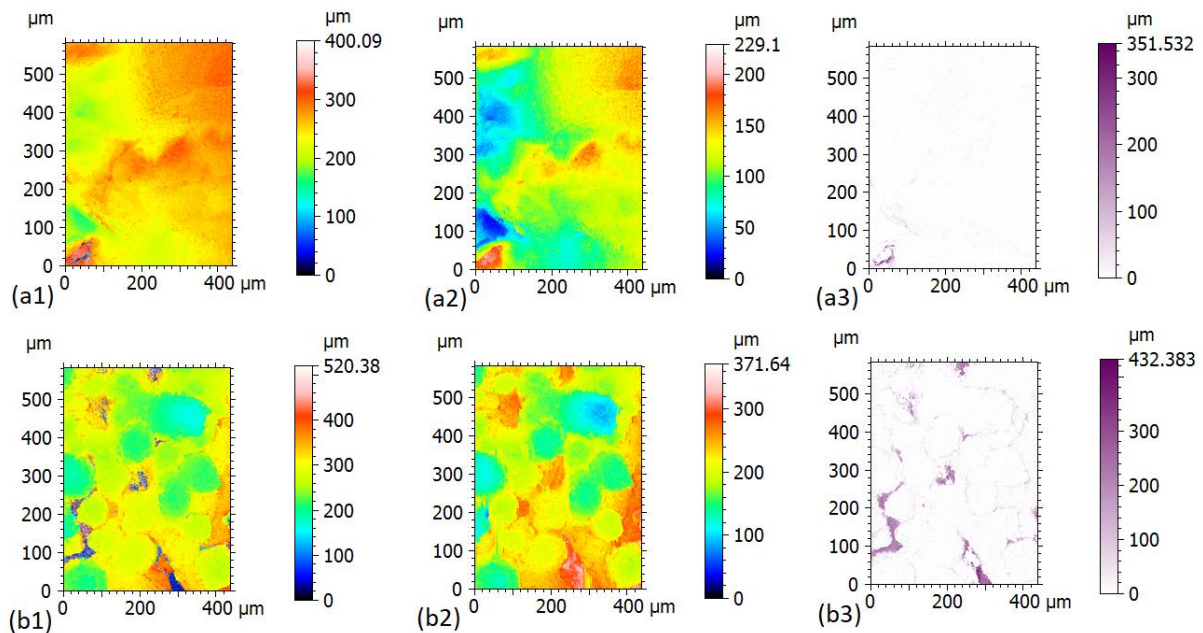

Figure 6. Comparison of topographies with respect to Rubert Microsurf 329 comparator test panel and MA with different methods: (a1) conventional method/MSS-25; (b1) conventional method/MA; (a2) proposed method/MSS-25; (b2) proposed method/MA; (a3) and (b3) show the differences between (a2) and (a1) as well as (b2) and (b1).

REFERENCES

[1] Tapia, G. and Elwany, A. A review on process monitoring and control in metal-based additive manufacturing. Journal of Manufacturing Science and Engineering. 136 (2014)

[2] Newton, L., Senin, N., Gomez, C., Danzl, R., Helmli, F., Blunt, L. & Leach, R. Areal topography measurement of metal additive surfaces using focus variation microscopy. Additive Manufacturing. 25 pp. 365-389 (2019)

[3] Townsend, A., Senin, N., Blunt, L., Leach, R. & Taylor, J. Surface texture metrology for metal additive manufacturing: a review. Precision Engineering. 46 pp. 34-47 (2016) 226

[4] Leach, R. Optical measurement of surface topography. (Springer, 2011) p. 227

[5] Danzl, R., Helmli, F. and Scherer, S. Focus variation – a robust technology for high resolution optical 3D surface metrology. Strojniški Vestnik-Journal of Mechanical Engineering. 57, 245-256 (2011)

[6] Tian, Y., Weckenmann, A., Hausotte, T., Schuler, A. and He, B. Measurement strategies in optical 3-D surface measurement with focus variation. Proceedings of 11th International Symposium on Laser Metrology for Precision Measurement and Inspection in Industry (ISCQM 2013). pp. 81-85 (2013)

[7] Giusca, C., Claverley, J., Sun,W., Leach, R., Helmli, F. and Chavigner, M. Practical estimation of measurement noise and flatness deviation on focus variation microscopes. CIRP Annals. 63, 545-548 (2014)

[8] Watanabe, M., Nayar, S. and Noguchi, M. Real time focus range sensor. IEEE Trans. Pattern Analysis and Machine Intelligence. 18, 1186-1198 (1996)

[9] Noguchi, M. and Nayar, S. Microscopic shape from focus using active illumination. Proceedings of 12th International Conference on Pattern Recognition. 1 pp. 147-152 (1994) 240

[10] Helmli, F. and Scherer, S. Adaptive shape from focus with an error estimation in light microscopy. ISPA 2001. Proceedings of the 2nd International Symposium on Image and Signal Processing and Analysis in Conjunction with 23rd International Conference on Information Technology Interfaces (IEEE Cat. pp. 188-193 (2001)

[11] Horii, A. The focusing mechanism in the KTH head eye system. (Citeseer, 1992)

[12] Martinez-Baena, J., Fdez-Valdivia, J. and García, J. A multi-channel autofocusing scheme for gray-level shape scale detection. Pattern Recognition. 30, 1769-1786 (1997)

[13] Nayar, S., Watanabe, M. and Noguchi, M. Real-time focus range sensor. IEEE Transactions on Pattern Analysis and Machine Intelligence. 18, 1186-1198 (1996)

[14] Nayar, S. and Nakagawa, Y. Shape from focus. IEEE Transactions on Pattern Analysis and Machine Intelligence. 16, 824-831 (1994)

[15] Xiong, Y. and Shafer, S. Depth from focusing and defocusing. Proceedings of IEEE Conference on Computer Vision and Pattern Recognition. pp. 68-73 (1993)

[16] Subbarao, M. and Choi, T. Accurate recovery of three-dimensional shape from image focus. IEEE Transactions on Pattern Analysis and Machine Intelligence. 17, 266-274 (1995)

[17] Pawlus, P., Reizer, R. and Wieczorowski, M. Comparison of results of surface texture measurement obtained with stylus methods and optical methods. Metrology and Measurement Systems. 25 (2018): 589-602

CONTACTS

Xin Xu   email: Xin.Xu@uni-kassel.de
Prof. Dr.-Ing. habil. Peter Lehmann   email: p.lehmann@uni-kassel.de
Hüseyin Serbes   email: h.serbes@uni-kassel.de
Tobias Pahl   email: tobias.pahl@uni-kassel.de